ELSEVIER

Physica A 239 (1997) 314–321

PHYSICA A

# Fractional Brownian motion of particles in capillary waves

Elsebeth Schröder*, Mogens T. Levinsen, Preben Alstrøm

*Center for Chaos and Turbulence Studies, The Niels Bohr Institute, Blegdamsvej 17, DK-2100 Copenhagen Ø, Denmark*

**Abstract**

On the surface of a vertically oscillating fluid, capillary waves with a clearly discernible wavelength $\lambda$ are formed if the amplitude of the oscillations exceeds a critical value. Particles sprinkled on the fluid surface are experimentally found to move in an almost Brownian motion when measured over distances larger than $\lambda$. We extend earlier studies of the diffusivity to length scales ranging from $0.1\lambda$ to $10\lambda$. We observe a cross-over in the diffusive motion from a strongly anomalous diffusion below $\lambda$, to a motion that is closer to being Brownian above $\lambda$. Our observations show that the particle motion is well described by an amplitude-independent fractional Brownian motion, effective at sizes less than $\lambda$, convoluted with an amplitude-dependent fractional Brownian motion, effective on all length scales smaller than the system size. At large amplitudes our results are in surprising agreement with diffusivity measurements from upper-ocean studies.

*PACS:* 47.20.Dr; 47.27.Qb; 05.40.+j; 47.52.+j

The motion of drifters near the sea surface has been a crucial element in probing oceanic turbulence [1]. Results obtained for the diffusivity by tracking drifters in the ocean show that the motion is far from being Brownian. In the geophysical dynamical regime [2], at time scales between roughly 1 day and 10 days and length scales between roughly 10 and 100km, the drifter motion possesses significant persistence ('memory'), which is not present in ordinary Brownian motion.

A similar persistence is observed for floating particles in laboratory experiments at length and time scales completely different from those of the oceanographic studies. The experiments reveal an outstandingly complex particle motion [3] that calls for more detailed studies of the transport properties. One such study was carried out by Ramshankar, Berlin and Gollub (RBG) [4], who measured the diffusivity for particles

* Corresponding author.


*PII* S0378-4371(97)00489-X

moving on capillary surface waves generated by the Faraday instability. To obtain the diffusivity, the particle displacement $\Delta x(\tau) = x(t + \tau) - x(t)$ over a time $\tau$ was measured along an arbitrary axis $x$ for many initiation times $t$. From the resulting distribution $P[\Delta x(\tau)]$ the variance $V(\tau)$ (mean square distance $\langle[\Delta x(\tau)]^2\rangle$) was found, and the diffusivity $D$ extracted; $V(\tau) = 2D\tau$. For Brownian motion, the diffusivity $D$ is a constant. RBG however found the diffusion to be slightly anomalous with a time-dependent diffusivity $D(\tau)$ that obeys a power law $D(\tau) = A\tau^{2H-1}$ on time scales larger than 1 s. The value of $H$ was observed to decrease gradually, from $H \simeq 0.7$ right above the Faraday instability to the value $H = 0.5$ (Brownian motion) at large wave amplitudes. As was pointed out by RBG, anomalous diffusion of this type can be modelled using a generalization of Brownian motion known as fractional Brownian motion [5]. We shall return to this point below.

The turbulence observed in surface waves is strongly influenced by the presence of a dispersion relation $\omega^2 = gk(1 + \frac{1}{2}a^2k^2)$ between the wave oscillation frequency (which equals half the driving frequency) and the wavelength $\lambda = 2\pi/k$ [6,7]. Here $g$ is the gravitational acceleration and $a$ is the capillary length of the fluid. At small frequencies (long wavelengths) the first term dominates, and the waves formed are called gravity waves (typical of ocean waves). At large frequencies (small wavelengths) the effect of gravity can be neglected, and the second term dominates. The waves thus formed are called capillary waves. These are the waves present in our experiment, where the observed wavelength is $\lambda = 2.6 \pm 0.1$ mm and the capillary length is $a = 3.1$ mm. Due to the dispersion relation we may expect that the diffusive behavior changes character at length scales comparable to $\lambda$. In this paper, we extend earlier studies of the diffusivity [4] in order to examine this point in detail. As we shall see, highly non-trivial dynamics is observed below the wavelength scale. Moreover, our observations of the diffusive motion are in surprising agreement with upper-ocean studies in the geophysical regime.

We have followed the motion of particles floating on a water surface in a cylindrical dish which was oscillated vertically so as to create capillary waves. The dish had an interior diameter of 8.4 cm and a height of 2 cm, and water filled the dish up to a height of approximately 1 cm. The dish was mounted on a frame fixed to a Brüel & Kjær vibration exciter type 4809, driven by a sinusoidal signal generated by a frequency synthesizer SRI model DS 345, operating at a frequency $f = 260$Hz. At this frequency the wavelength was observed to be $\lambda = 2.6 \pm 0.1$ mm. The vibration amplitude $\mathscr{A}$ of the vertical oscillations is proportional to the voltage applied to the exciter, and this voltage was the actual control parameter in the experiments. The particles used were mushroom spores, chosen because of their small mass and size (approximately 50 μm), and their strong resistance to being wetted by water, assuring that they will float. A CCD camera recorded the images of the particles on a VCR tape, and the output of the VCR was fed into a frame grabber board in a personal computer. At vibration amplitudes $\mathscr{A}$ right above the critical amplitude $\mathscr{A}_c$ at which surface waves are first formed, a square pattern with moving defects is observed. However, when $\mathscr{A}$ is increased to 10% or more above $\mathscr{A}_c$, the defects dominate and the wave pattern becomes random in appearance.

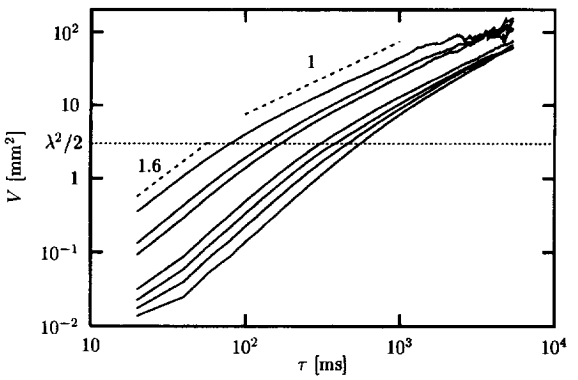


Fig. 1. Variance $V$ (mean square distance $\langle[\Delta x(\tau)]^2\rangle$) obtained along one coordinate axis as a function of the time interval $\tau$. From below, $\varepsilon = 0.05, 0.13, 0.24, 0.34, 0.65, 0.86$, and 1.06. The dashed top lines are straight lines with slopes 1.6 and 1.0, respectively.

The horizontal positions of the particles were measured at 20 ms intervals, and in each of two orthogonal coordinate directions the variance $V(\tau)$ was calculated for time intervals $\tau$ ranging from 20 ms to approximately 5000 ms, limited by the fact that the particles eventually move outside the camera window (which is circular with a radius of 3 cm $\approx$ 70% of the dish radius). The variance was obtained for seven different amplitudes of vibration (Fig. 1). In terms of the reduced control parameter $\varepsilon = (\mathscr{A} - \mathscr{A}_c)/\mathscr{A}_c$, we consider $\varepsilon = 0.05$, 0.13, 0.24, 0.34, 0.65, 0.86, and 1.06. For each value of $\varepsilon$, the variance was calculated from a sample of $\sim 1000$ particle tracks, each having $\sim 100$ observation points separated by 20 ms in time. For both $\varepsilon$ large and $\tau$ large, the sample was somewhat smaller, giving rise to noisy fluctuations, see Fig. 1. The obtained distribution of displacements, $P[\Delta x(\tau)]$, did not differ in the two orthogonal directions, indicating that there was no preference for any spatial direction in the horizontal plane.

We find that all seven curves in Fig. 1 show a cross-over at an $\varepsilon$-dependent time $\tau = \tau_c(\varepsilon)$, with one power-law behavior for large times, $V(\tau) = 2A\tau^{2H}$, and a *steeper* power-law behavior $V(\tau) \sim \tau^{2H'}$ at small time scales. At $\varepsilon = 0.05$ and $\varepsilon = 0.13$ the curve bends towards a smaller slope at very small distances. This bending, however, is a consequence of the uncertainty in position caused by the finite pixel size.

First we notice that the cross-over is located where $2V(\tau) \simeq \lambda^2$ (recall that $V$ only refers to the displacement in one direction). In Fig. 2 the cross-over time $\tau_c$ is shown as a function of $\varepsilon$. We find that $\tau_c$ falls off exponentially with $\varepsilon$. Furthermore, as $\varepsilon$ approaches zero, the value of $\tau_c$ tends to a constant $\tau_c \approx 600$ ms. We find this time to be much smaller (a couple of magnitudes) than the time it takes the mushroom spores to diffuse the distance $\lambda = 2.6$ mm when no surface waves are present. The transition at $\varepsilon = 0$ where wave oscillations emerge is thus associated with a significant jump in the diffusivity.

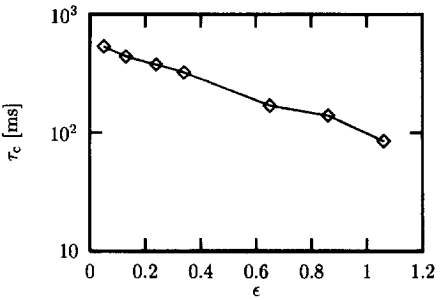


Fig. 2. The cross-over time $\tau_c(\varepsilon)$, determined from Fig. 1.

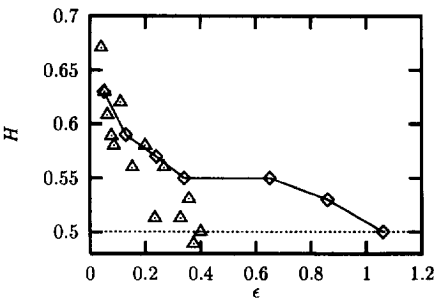


Fig. 3. The exponent $H$ characterizing the long-time behavior, as a function of $\varepsilon$. Diamonds are our measurements of the slopes $(2H)$ in Fig. 1 for large time scales. Triangles are measurements by Ramshankar et al. [4].

Next, consider the long-time behavior at lengths larger than the wavelength. In accordance with the measurements by RBG [4] we find that the exponent $2H$ for the variance decreases with $\varepsilon$ with the most anomalous diffusion at low $\varepsilon$ ($2H = 1.26$ for $\varepsilon = 0.05$), while Brownian diffusion ($2H = 1.0$) is obtained at the largest oscillation amplitude, $\varepsilon = 1.06$. The dependence of the exponent $H$ on $\varepsilon$ is shown in Fig. 3. Also shown are the values of $H$ obtained by RBG (although indirectly obtained as a roughness exponent). The decrease of $H$ with $\varepsilon$ towards $H = \frac{1}{2}$ appears to be slower in our experiment.

We find the pre-factor $A = A(\varepsilon)$ in the diffusivity to be roughly a factor of two larger than the amplitudes found by RBG (Fig. 4). We believe this is due to the larger size of particles used by RBG (diameter 100–200 μm, compared to our mushroom spores of size $\sim 50\,\mu m$). The pre-factor seems to grow exponentially with $\varepsilon$. From the relation $2A(\varepsilon)[\tau_c(\varepsilon)]^{2H(\varepsilon)} \simeq (\lambda^2/2)$, the exponential dependence follows as a consequence of the exponential decay of the cross-over time $\tau_c$ with $\varepsilon$ (since $H(\varepsilon)$ is a slowly varying function of $\varepsilon$). In analogy with $\tau_c$, a significant change in $A$ is expected at $\varepsilon = 0$.

At short time scales, corresponding to length scales shorter than the wavelength, the slopes $2H_<$ are found to be larger than $2H$, the latter being the exponent characterizing the long-time behavior. We find that $2H_<$ decreases from $\approx 1.9$ to 1.6 in the range of $\varepsilon$

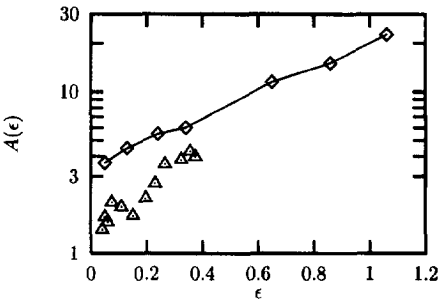


Fig. 4. Amplitude $A(\varepsilon)$ of the diffusivity $D(\tau)=A\tau^{2H-1}$. The unit of $A$ is $[A]=\mathrm{mm}^2\,\mathrm{s}^{-2H}$. Diamonds are our measurements, triangles are measurements by Ramshankar et al. [4].

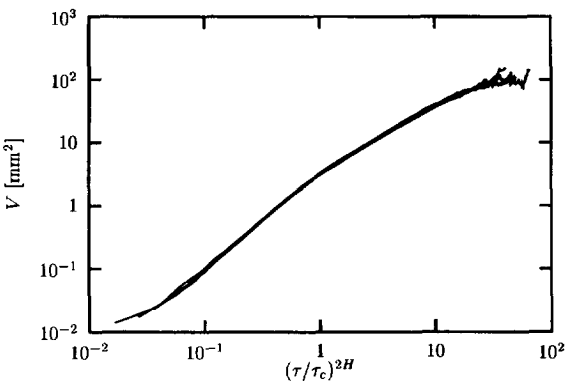


Fig. 5. The curves from Fig. 1 are collapsed into one scaling function, by means of a rescaling of time. See the text for details.

studied. Moreover, the ratio of the exponents for short and long time scales, $\gamma \equiv H_\lambda/H$, is very close to being a constant, i.e. *independent* of $\varepsilon$. We find $\gamma = 1.55 \pm 0.05$. This result suggests that the $\varepsilon$ dependence can be removed by a proper rescaling of the time. In Fig. 5, a surprisingly good data collapse is obtained for the seven curves of Fig. 1 by rescaling time, $\tau \to \tau' = [\tau/\tau_c(\varepsilon)]^{2H(\varepsilon)}$. Fig. 5 shows that the variance is an $\varepsilon$-independent function of the rescaled time, $V = f(\tau')$. The scaling function $f$ reflects the cross-over in the dynamical behavior at $f(1) = \lambda^2/2$. We have $f(\tau') \sim \tau'^{\gamma}$ below the cross-over ($\gamma = 1.55 \pm 0.05$), and $f(\tau') \sim \tau'$ above.

The separation of the cross-over from the $\varepsilon$-dependence is further emphasized by plotting the variance $V$ for the various $\varepsilon$ values versus the variance for a particular $\varepsilon$ value, using the reduced time $\tau/\tau_c(\varepsilon)$ as the parameter (Fig. 6). We have chosen $\varepsilon = 1.06$ as the reference (having ordinary Brownian motion at $\tau > \tau_c$). As is observed, there is no sign of $\lambda$; all curves are straight lines. The slopes are $2H(\varepsilon)$ [since $2H(\varepsilon = 1.06) = 1.0$]. We stress that the approach toward Brownian motion as the amplitude is increased is

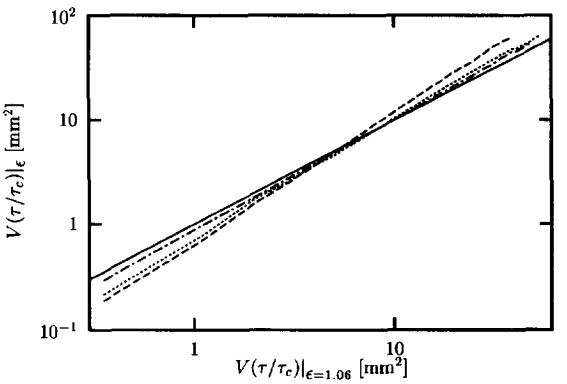


Fig. 6. The variance $V$ for $\varepsilon = 0.05$ (dashed line), $\varepsilon = 0.24$ (dotted line), and $\varepsilon = 0.65$ (dash-dotted line), plotted versus the variance for $\varepsilon = 1.06$, using the reduced time $\tau/\tau_c(\varepsilon)$ as the parameter. For comparison, a line of slope 1 is shown (unbroken line).

*not* an effect of a correlation length $\xi$ that gradually decreases from the system size to the wavelength. This would give rise to a cross-over at $\xi$, and there is no sign of such a length scale in our measurements.

Fig. 6 illustrates the deviations from Brownian motion at long time scales, and it clearly shows the $\varepsilon$-dependent persistence or 'memory' possessed by the particles on all time scales studied. This behavior can be modelled by a so-called *fractional* Brownian motion, which is a generalized form of Brownian motion. In ordinary Brownian motion the displacement $\Delta x(\tau) = x(t+\tau) - x(t)$ is characterized by a Gaussian distribution, $P(s) \sim \exp(-s^2)$, with $s = \Delta x(\tau)/\tau^{1/2}$. For fractional Brownian motion, the Gaussian-distributed quantity is $s' = \Delta x(\tau)/\tau^H$, where $H \neq \frac{1}{2}$. This immediately introduces infinite-time correlations. While for ordinary Brownian motion, two successive displacements $x(t) - x(t - \tau_1)$ and $x(t + \tau_2) - x(t)$ are independent, one finds that this is not so for fractional Brownian motion. The correlation between two successive displacements is

$$
\begin{aligned}
C(\tau_1, \tau_2) &= \left\langle \frac{[x(t) - x(t-\tau_1)]}{\tau_1^H} \, \frac{[x(t+\tau_2) - x(t)]}{\tau_2^H} \right\rangle \\
&= \frac{1}{2(\tau_1\tau_2)^H} \{ \langle [x(t+\tau_2) - x(t-\tau_1)]^2 \rangle - \langle [x(t+\tau_2) - x(t)]^2 \rangle \\
&\quad - \langle [x(t) - x(t-\tau_1)]^2 \rangle \} \\
&\propto \frac{[(\tau_1+\tau_2)^{2H} - \tau_1^{2H} - \tau_2^{2H}]}{(\tau_1\tau_2)^H} \, . \qquad (1)
\end{aligned}
$$

For $\tau_1 = \tau_2 = \Delta t$, we have $C \propto 2^{2H} - 2$, which is non-zero for $H \neq \frac{1}{2}$ and is independent of the size of the time interval $\Delta t$ considered, indicating the strong memory of all past displacements.

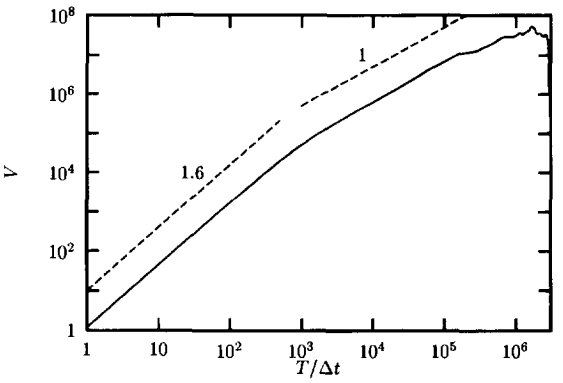


Fig. 7. Simulation of a fractional Brownian motion with a cut-off time introduced at $T/\Delta t = 600$.

From Eq. (1) we can also calculate the correlation between two displacements separated in time by $T \gg \Delta t$,

$$
\begin{aligned}
C_T &= \left\langle \frac{[x(t+\Delta t)-x(t)]}{\Delta t^H} \, \frac{[x(t+T+\Delta t)-x(t+T)]}{\Delta t^H} \right\rangle \\
&= \frac{1}{\Delta t^{2H}} \{ -\langle [x(t+T)-x(t+\Delta t)][x(t+T+\Delta t)-x(t+T)] \rangle \\
&\quad + \langle [x(t+T)-x(t)][x(t+T+\Delta t)-x(t+T)] \rangle \} \\
&\propto \left(\frac{T}{\Delta t}\right)^{2H} \left\{ -2 + \left(1-\frac{\Delta t}{T}\right)^{2H} + \left(1+\frac{\Delta t}{T}\right)^{2H} \right\} \\
&\simeq H(2H-1)\left(\frac{T}{\Delta t}\right)^{2H-2} . \qquad (2)
\end{aligned}
$$

A cut-off time for the memory of the fractional Brownian motion can be introduced. At time scales larger than this cut-off time, the motion again becomes ordinary Brownian. In Fig. 7 the variance is computed for a fractional Brownian motion with $H = 0.8$ and a 'memory' time limit of $T/\Delta t = 600$. As is observed, the cross-over from fractional to ordinary Brownian motion at $T/\Delta t \simeq 600$ is apparent in the variance.

The strong resemblance between Figs. 7 and 5 suggests that the diffusion may be modelled by a convolution of two fractional Brownian motions: an *ε-independent* motion effective below the wavelength (Fig. 5), convoluted with an *ε-dependent* motion which is effective on all length scales smaller than the system size (Fig. 6). In physical terms, the former may result from turbulent eddies of size less than the wavelength, while the latter results from turbulent eddies of all sizes less than the system size. One may speculate that our way of plotting the data can be useful in a more general context of turbulence, e.g. where the Reynolds number replaces $\varepsilon$.

Our observations of particle trajectories may be compared with upper-ocean studies of drifter motion. In the geophysical regime corresponding to time scales between roughly 1 day and 10 days, and length scales between roughly 10 and 100 km, drifter

diffusion has been studied in the North Atlantic [8–10]. From the observations they find a fractional Brownian drifter motion with a well-defined exponent $2H_g = 1.5$. The same exponent ($2H_g = 1.4$–$1.6$) is found from data obtained for drifters in the Kuroshio extension (oceanographic location off the coast of Japan) [1]. For scales larger than 100–200 km [2], the dynamics is essentially governed by Rossby waves [11] and zonal flows, and a cross-over to ordinary Brownian motion is observed with exponent $2H = 1$. Thus, the diffusion may be modelled by a fractional Brownian motion effective below roughly 100 km.

It is noteworthy that the value of $H_g$ does not vary geographically, and that the value is the same as the value of $H_\lambda$ found in our laboratory experiment at large wave amplitudes. There the motion also exhibits a cross-over from fractional to ordinary Brownian motion. This suggests that the exponent $2H_g = 2H_\lambda = 1.4$–$1.6$ is intrinsic to the eddy turbulence governing near-surface motion at a variety of scales, ranging from several km in the upper-ocean to mm scales in capillary ripples.

In summary, measurements of the diffusivity in capillary waves suggest that the turbulent surface motion can be modelled by a convolution of a fractional Brownian motion, generated by eddies of the size of the wavelength or less, with another fractional Brownian motion, effective on all length scales smaller than the system size. At large wave amplitudes, the latter motion approaches ordinary Brownian motion. In this case, the diffusive motion changes from a fractional Brownian motion with exponent $2H_\lambda = 1.6$ on small length scales to ordinary Brownian motion with $2H = 1$ on large length scales. These exponents are identical to those found in upper-ocean studies, where the cross-over is observed at 100 km scales, not mm scales.

We have profited greatly from discussions with W. Goldburg. This work was supported by the Novo-Nordisk Foundation and by the Danish Natural Science Research Council.

## References

[1] See e.g. A. Provenzale, A.R. Osborne, A.D. Kirwan Jr. and L. Bergamasco, in: Nonlinear Topics in Ocean Physics, ed. A.R. Osborne (North-Holland, Amsterdam, 1991) p. 367.
[2] A.R. Osborne, A.D. Kirwan Jr., A. Provenzale and L. Bergamasco, Tellus A 41 (1989) 5.
[3] See e.g. M. Van Dyke, An Album of Fluid Motion (Parabolic, Stanford, CA, 1982).
[4] R. Ramshankar, D. Berlin and J.P. Gollub, Phys. Fluids A 2 (1990) 1955.
[5] See e.g. B.B. Mandelbrot, The Fractal Geometry of Nature (Freeman, San Francisco, 1982).
[6] V.E. Zakharov, V.S. L'vov and G. Falkovich, Kolmogorov Spectra of Turbulence I (Springer, Berlin, 1992).
[7] E. Schröder, J.S. Andersen, M.T. Levinsen, P. Alstrøm and W.I. Goldburg, Phys. Rev. Lett. 76 (1996) 4717.
[8] A.C. de Verdiere, J. Mar. Res. 41 (1983) 375.
[9] D.A. Booth, Deep-sea Res. 35 (1988) 1937.
[10] B.G. Sanderson and D. Booth, Tellus A 43 (1991) 334.
[11] D.J. Tritton, Physical Fluid Dynamics (Clarendon Press, Oxford, 1988).